Origin of Low-Frequency Dielectric Permittivity In $BiFeO_3$ Multiferroic Ceramics

C.-S. Tu* and T.-H. Wang
Graduate Institute of Applied Science and Engineering
Fu Jen Catholic University
Taipei 242, Taiwan
039611@mail.fju.edu.tw

V. H. Schmidt and R. R. Chien
Department of Physics
Montana State University
Bozeman, Montana 57917, USA
schmidt@physics.montana.edu

***Abstract*—A one-dimensional conductivity barrier model is introduced to describe the dielectric response and conductivity of $BiFeO_3$ (BFO) and $(Bi_{0.95}Nd_{0.05})FeO_3$ (BFO-5%Nd) ceramics as functions of temperature and frequency. Good qualitative fits of conductivity and dielectric permittivity in the intermediate-temperature region (500-800 K) are obtained with intrinsic barriers of B=8700 K (for BFO) and B=8400 K (for BFO-5%Nd), and extrinsic barriers of Δ=2500 K (for BFO and BFO-5%Nd). The phase-shifted conductivity is responsible for a step-like dielectric relaxation in the region of 500-800 K. The experimental conductivity departs from the conductivity-barrier-model fit below 650 K. This deviation is likely caused by the magneto-electric coupling near the antiferromagnetic-paramagnetic transition. This work suggests that the 5% mole Nd-substitution can stabilize the perovskite structure in BFO ceramic.**

Keywords-component; $BiFeO_3$; dielectric permittivity; barrier model; magneto-electric coupling

I. INTRODUCTION

Multiferroic materials enable a coupling interaction between ferromagnetic (FM) and ferroelectric (FE) parameters. This magnetoelectric coupling can be utilized to develop additional functionalities that induce magnetization using external electric field or FE polarization using external magnetic field. The multiferroic BFO is perhaps the only material that possesses both magnetic and FE properties at and above room temperature. BFO has a high antiferromagnetic (AFM)—paramagnetic (PM) Néel temperature at T_N=352-397 ^oC and FE Curie temperature at T_C=810-870 ^oC [1,2]. A $R3c$ rhombohedral structure (a_R=5.616 Å and α_R=59.35^o) was reported for bulk BFO [3], and can also be indexed based on the pseudo-cubic lattice (a_p=3.96 Å) [4]. The neutron diffraction suggested a FE rhombohedra—paraelectric (PE) orthorhombic transition at $T_C \cong 820$ ^oC in BFO [5,6].

It has been a challenge to synthesize single-phase BFO ceramics with considerable electric polarization due to current leakage and second phases [7,8]. To enhance FM and FE features, many studies have focused on BFO ceramics with substituted ions in the A or B sites of the perovskite structure [9-11]. A-site substitutions of rare-earth cations are expected to suppress the spiral magnetic modulation and enhance a FM response [6].

$NdFeO_3$ is known to be orthorhombic structure with a G-type AFM Néel temperature (T_N) at 487 ^oC [12]. From x-ray diffraction (XRD), orthorhombic and triclinic structures were proposed in $Bi_{1-x}Nd_xFeO_3$ ceramics for x=0.4-1.0 and x=0.2, respectively [12]. Triclinic and pseudo-tetragonal structures were proposed in $Bi_{1-x}Nd_xFeO_3$ for x=0.05-0.15 and x=0.175-0.20, respectively [13]. An XRD result revealed a first-order AFE orthorhombic (*Pnam*) — PE orthorhombic (*Pbnm*) transition in $Bi_{1-x}Nd_xFeO_3$ ceramics for $0.10 \le x \le 0.25$ [6].

II. EXPERIMENTAL

The $BiFeO_3$ (BFO) and $(Bi_{0.95}Nd_{0.05})FeO_3$ (BFO-5%Nd) ceramics were prepared by the solid state reaction method. For synthesis of BFO, Bi_2O_3 and Fe_2O_3 powders (purity ≥ 99.0%) were weighed in 1:1 molar ratio and then mixed in an agate mortar for more than 24 hrs using alcohol as a medium. The mixture was dried before calcining at 800 ^oC for 3 hrs. The calcined powder was mixed with polyvinyl acetate as a binder for granulation, and was then pressed into a 1.0 cm-diameter disk for sintering at 750 ^oC for 1 hr. For BFO-5%Nd ceramic, Bi_2O_3, Nd_2O_3, and Fe_2O_3 powders were weighed in a 0.95:0.05:1 ratio. The calcined powder was sintered at 860 ^oC for 2 hr. The real (ε') and imaginary (ε'') parts of dielectric permttivity were obtained by measuring capacitance and resistance with a Wayne-Kerr Analyzer PMA3260A.

III. RESULTS AND DISCUSSION

Figure 1 shows X=ray diffraction spectra of BFO and BFO-5%Nd ceramics at room temperature. BFO and BFO-5%Nd show a similar XRD spectrum and have a rhombohedral structure. Very minor second phases occur in BFO and BFO-5%Nd, and are possible $Bi_{25}FeO_{39}$ or $Bi_2Fe_4O_9$ as indicated by "*" [3]. BFO-5%Nd exhibits less second phase, suggesting that the Nd-substitution can stabilize the perovskite structure. The XRD peaks of BFO–5%Nd occur at slightly higher 2θ than those in BFO, due to the smaller atomic radius of the Nd^{3+} ion (1.12 Å) compared with the Bi^{3+} ion (1.17 Å) on the perovskite A site.

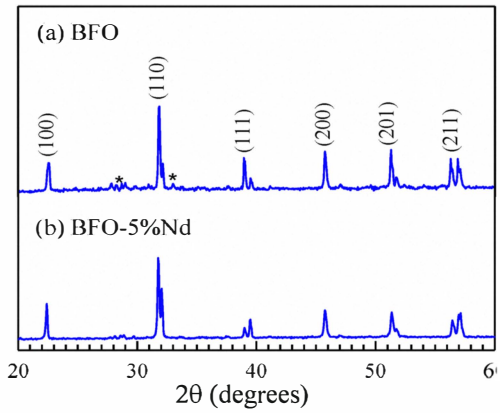

Fig. 1 XRD spectra of (a) BFO and (b) BFO-5%Nd ceramics at room temperature.

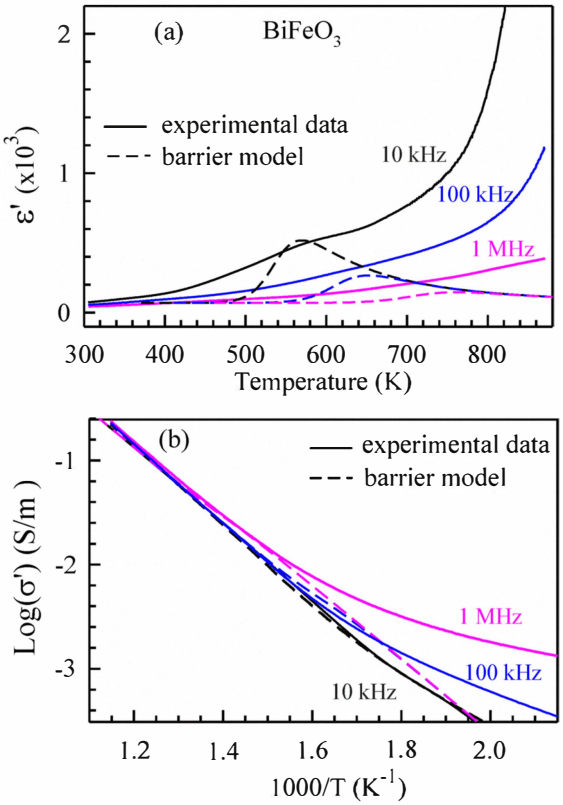

Fig. 2 (a) ε' and ε'', and (b) conductivity σ' of BFO. The barrier-model fits of σ' and ε' are given in (b) and (a). The fitting parameters are: $\varepsilon'_\infty = 70$, d=30 nm, B=8700 K, Δ =2500 K, and $n = 6.0\times10^{26}/m^3$.

Figures 2 and 3 display dielectric permittivity, conductivity, and model fits for BFO and BFO-5%Nd. The ε' of BFO and BFO-5%Nd are respectively about 75 and 90 at room-temperature for f=10 kHz. The low-temperature shoulder feature in ε' at low frequency is more pronounced for BFO-5%Nd than for BFO. At higher temperatures a phase-shifted conductivity is evident, while at lower temperatures a permittivity feature not associated with conductivity dominates. The nearly Arrhenius behavior at higher temperature, plotted as log σ' *vs.* $10^3/T$ using the relation $\varepsilon'' = \sigma'/\varepsilon_o\omega$ in Figs. 2(b) and 3(b), is the major effect of this conductivity mechanism. The phase shift of this conductivity also causes a step-like dielectric dispersion in 500-800 K for f=10 kHz-1 MHz. The $\varepsilon'/\varepsilon''$ ratio in the high temperature range (> 600 K) is about 0.01-0.1, and corresponds to a conductivity phase shift of only a few degrees.

To understand the large conductivity and dielectric response in the high-temperature region, a one-dimensional barrier model was derived as illustrated in Fig. 4, in which B represents the intrinsic barriers spaced a distance a apart, where a is of the order of a lattice constant. B+Δ are extrinsic barriers spaced a distance d apart. The attempt frequency for crossing the barriers is $\nu = k\Theta/h$, where k, Θ, and h are the Boltzmann constant, Debye temperature, and Planck's constant. We chose Θ=300 K in this calculation. The complex ac conductivity $\sigma(\omega,T) = \sigma'+i\sigma''$ can be defined as;

$$\sigma(\omega,T) = (J + \partial D/\partial t)/\langle E\rangle \equiv J_t/\langle E\rangle \qquad (1)$$

J and $\partial D/\partial t$ are position-dependent conduction current density and displacement current density, but J_t is independent of position as required by electrodynamics. <*E*> is the spatially averaged measured field.

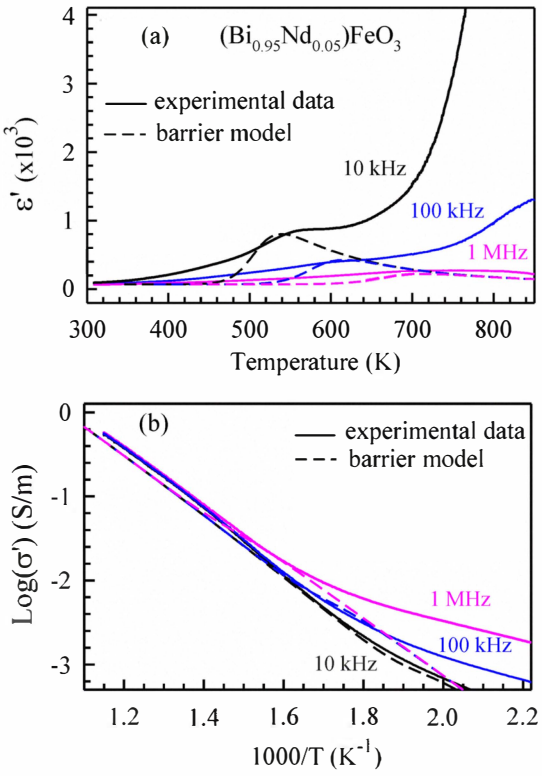

Fig. 3 (a) ε' and ε'', and (b) conductivity σ' of BFO-5%Nd. The barrier-model fits of σ' and ε' are given in (b) and (a). The fitting parameters are: $\varepsilon'_\infty = 70$, d=20 nm, B=8400 K, Δ =2500 K, and $n = 1.0\times10^{27}/m^3$.

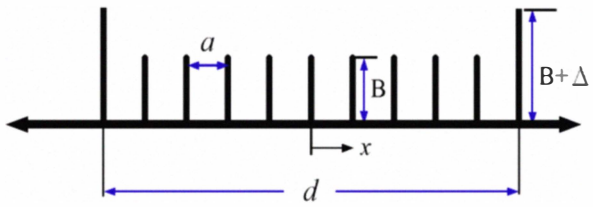

Fig. 4 One-dimensional barrier model with intrinsic barriers B at spacing *a*, and extrinsic barriers B+Δ at spacing *d*.

We assume conductivity with a temperature-independent carrier density *n* and carrier charge *q*=2e for oxygen vacancy carriers, or ± *e* for hole or electron hopping conductivity carriers. The $\sigma_\infty = J/E$, taking into account that the number of carrier per unit area in a unit-cell layer on either side of a barrier layer is *na* and their attempt frequency for crossing the barrier is ν, can be expressed by;

$$\sigma_\infty = q\nu na[e^{(-kB+\frac{1}{2}qEa)/kT} - e^{(-kB-\frac{1}{2}qEa)/kT}]/E \cong (nq^2a^2\Theta/hT)e^{-B/T} \quad (2)$$

Using the Gauss law $\partial D/\partial x = \rho$ and the diffusion equation $\partial\rho/\partial t = \overline{D}\nabla^2\rho$, Eq. (1) becomes

$$J = \sigma_\infty E - \overline{D}\partial\rho/\partial x = \sigma_\infty E - \sigma_\infty\tau(\partial\rho/\partial x) \quad (3)$$

$\overline{D}$ and ρ are diffusion coefficient and charge density. The Einstein relation $q\overline{D} = \mu kT = (v_d/E)kT$, $\tau = kT/(nq^2)$ and $\sigma_\infty = nq\mu = nq(v_d/E)$ were used in Eq. (3). v_d is the drift velocity. Taking the *x* derivative of Eq. (3), we have

$$\partial E/\partial x = (\partial J/\partial x)/\sigma_\infty + \tau(\partial^2\rho/\partial x^2) \quad (4)$$

To eliminate *J* and *E*, the one-dimensional Gauss's law $\partial E/\partial x = \rho/\varepsilon_\infty$ and continuity equation $\partial J/\partial x = -\partial\rho/\partial t$ were used in Eq. (4), then

$$\partial^2\rho/\partial x^2 - \rho/(\tau\varepsilon_\infty) - (\partial\rho/\partial t)/(\tau\sigma_\infty) = 0 \quad (5)$$

This equation is separable and we may assume $\rho(x,t) = f(x)e^{i\omega t}$. Then Eq. (5) becomes

$$(\partial^2 f/\partial x^2) - \alpha^2 f = 0 \text{ and } \alpha^2 = 1/(\tau\varepsilon_\infty) + i\omega/(\tau\sigma_\infty) \quad (6)$$

The solution is $f(x) = Ae^{\alpha x} + Be^{-\alpha x}$. For a neutral material, $\rho(x=0)=0$ at the mid-point between higher barriers is expected, i.e. *B*=-*A*. Then $\rho(x,t)$ becomes $\rho(x,t) = A'\sinh(\alpha x)e^{i\omega t}$. From here on, the time dependence $e^{i\omega t}$ will be omitted in expressions for ρ, *J*, and *E*.

From Eq. (3), the current density *J* at $x=d/2$ can be expressed by

$$J(d/2) = \sigma_\infty[E(d/2) - \tau(\partial\rho/\partial x)]e^{-\Delta/T} \quad (7)$$

The difference in carrier density across the higher barriers is

$$\rho(d/2) - \rho(-d/2) = 2\rho(d/2),\ \partial\rho/\partial x \cong 2\rho(d/2)/a \quad (8)$$

Thus,

$$J(\pm d/2) = \sigma_\infty\{E(\pm d/2) - \tau[\rho(-d/2) - \rho(d/2)]/a\}e^{-\Delta/T} = \sigma_\infty e^{-\Delta/T}\{E(\pm d/2) + 2\tau a^{-1}A'\sinh(b)\} \quad (9)$$

where $b = \alpha d/2$. Using Eq. (3) and $\partial\rho/\partial x = A'\alpha\cosh(\alpha x)$, we obtain

$$E(\pm d/2) = \tau A'[2a^{-1}e^{-\Delta/T}\sinh(b) + \alpha\cosh(b)](1 - e^{-\Delta/T})^{-1} \quad (10)$$

Then Eq. (9) becomes

$$J(\pm d/2) = \sigma_\infty\tau A'e^{-\Delta/T}[\alpha\cosh(b) + 2a^{-1}\sinh(b)](1 - e^{-\Delta/T})^{-1} \quad (11)$$

From Eqs. (10) and (11), we can determine the total current,

$$J_t = \tau A'e^{-\Delta/T}\{\sigma_\infty[\alpha\cosh(b) + 2a^{-1}\sinh(b)] + i\omega\varepsilon_\infty[2a^{-1}\sinh(b) + e^{\Delta/T}\alpha\cosh(b)]\}(1 - e^{-\Delta/T})^{-1} \quad (12)$$

The electric field *E* in the interval $-d/2 < x < d/2$, can be obtained by

$$E(x) = \int\rho(x)dx/\varepsilon_\infty = E(-d/2) + (A'/\varepsilon_\infty)\int_{-d/2}^{x}\sinh(\alpha x)dx \quad (13)$$

Then, the average field $<E>$ can be calculated by

$$\langle E\rangle = \frac{1}{d}\int_{-d/2}^{d/2}E(x)dx$$

By using Eqs. (1), (12), and (13) carrying out considerable calculation, we obtain

$$\sigma(\omega,T) = \{\sigma_\infty e^{-\Delta/T}[2a^{-1}\sinh(b) + \alpha\cosh(b)] + i\omega\varepsilon_\infty[2a^{-1}e^{-\Delta/T}\sinh(b) + \alpha\cosh(b)]\} \times\{2a^{-1}e^{-\Delta/T}\sinh(b) + \alpha\cosh(b) + (2/d\tau\varepsilon_\infty\alpha^2)[\sinh(b) - b\cosh(b)](1 - e^{-\Delta/T})\}^{-1} \quad (14)$$

α and b are complex. The permittivity $\varepsilon(\omega,T)=\varepsilon'-i\varepsilon''$ is related to σ by $\varepsilon'=\sigma''/\varepsilon_o\omega$ and $\varepsilon''=\sigma'/\varepsilon_o\omega$.

As shown by the dashed lines in Figs. 2(b) and 3(b), the conductivities $\sigma'(\omega,T)$ of BFO and BFO-5%Nd were fitted fairly well in the high-temperature region by using Eq. (14), from which parameters of ε_∞', n, d, B, and Δ were obtained. The lattice constant of a=0.398 nm was calculated from the XRD (Fig. 1). The slight gap between the barrier-model fits and experimental σ' in the high-temperature region (> 700 K) may be attributed to higher-barrier conductivity and/or electronic conductivity, which cause an upturn in ε'.

The conductivity begins to depart from the barrier-model fit near 650 K for f=1 MHz. This deviation is likely caused by the magneto-electric coupling [1-2]. The synchrotron XRD of BFO revealed a minimum in rhombohedral angle α_R near 670 K, due to the changes in positions of Bi^{3+} and Fe^{3+} ions [14], and this temperature is near the range of the permittivity step. The n=6.0×10^{26}/m^3 for BFO and n=1.0×10^{27}/m^3 for BFO-5%Nd are smaller than n=1.5×10^{27}/m^3 in $SrTiO_3$ [15].

The solid curves in Figs. 2(a) and 3(a) are fits of ε' for f =10 kHz- 1 MHz by using Eq. (14) and parameters acquired from the fits of conductivities σ'. The barrier model can qualitatively describe the step-like relaxation behavior with dielectric maxima in the range of 500-800 K. The slight discrepancy between the barrier-model fits and ε' data could be due to having both ionic and electronic conductivities, and to higher barriers actually having distributions of spacings d and heights.

In conclusion, the conductivity-barrier model can qualitatively describe the large conductivities and dielectric responses of BFO and BFO-5%Nd ceramics. BFO has a higher intrinsic barrier B than BFO-5%Nd, indicating 5%mole Nd-substitution can enhance conductivity. The spacing distances d=30 and 20 nm of extrinsic barriers were estimated for BFO and BFO-5%Nd ceramics, respectively. A step-like dielectric relaxation in the 500-800 K range in BFO and more strongly in BFO-5%Nd, is caused by the phase-shifted conductivity. The conductivities depart from the barrier-model fits below 650 K and are likely caused by the magneto-electric coupling.

ACKNOWLEDGMENT

This work was supported by National Science Council of Taiwan Grant No. 97-2112-M-030-003-MY3.

References

[1] P. Fischer, M. Polomska, I. Sosnowska, and M. Szymański, "Temperature Dependence of the Nuclear and Magnetic Structure of $BiFeO_3$," J. Phys. C , vol. 13, pp. 1931-1940, 1980.

[2] B. Ramachandran and M.S. Ramachandra Rao, "Low temperature magnetocaloric effect in polycrystalline $BiFeO_3$ ceramics," Appl. Phys. Lett., vol. 95, pp. 142505 (3 pages), October 2009.

[3] F. Kubel and H. Schmid, "Structure of a ferroelectric and ferroelastic monodomain crystal of the perovskite $BiFeO_3$," Acta Crystallogr., Sect. B: Structure Science, vol. 46, pp. 698-702, 1990.

[4] J. Li, J. Wang, M. Wuttig, R. Ramesh, N. Wang, B. Ruette, A. P. Pyatakov, A. K. Zvezdin, and D. Viehland, "Dramatically enhanced polarization in (001), (101), and (111) $BiFeO_3$ thin films due to epitiaxial-induced transitions," Appl. Phys. Lett., vol. 84, 5261 (3 pages), June 2004.

[5] D.C. Arnold, K.S. Knight, F.D. Morrison, and P. Lightfoot, ", Ferroelectric-Paraelectric Transition in $BiFeO_3$: Crystal Structure of the Orthorhombic β Phase" Phys. Rev. Lett., vol. 102, pp. 027602 (4 pages), January 2009.

[6] I. Levin, S. Karimi, V. Provenzano, C.L. Dennis, H. Wu, T.P. Comyn, T.J. Stevenson, R.I. Smith, and I.M. Reaney, "Reorientation of magnetic dipoles at the antiferroelectric-paraelectric phase transition of $Bi_{1-x}Nd_xFeO_3$ ($0.15\leq x\leq 0.25$)," Phys. Rev. B, vol. 81, pp. 020103(R) (4 pages), January 2010.

[7] R. Palai, R.S. Katiyar, H. Schmid, P. Tissot, S.J. Clark, J. Robertson, S.A.T. Redfern, G. Catalan, and J.F. Scott, "β phase and γ-β metal-insulator transition in multiferroic $BiFeO_3$," Phys. Rev. B, vol. 77, pp. 014110 (11 pages), January 2008.

[8] S.T. Zhang, M.H. Lu, D. Wu, Y.F. Chen, and N.B. Ming, "Larger polarization and weak ferromagnetism in quenched $BiFeO_3$ ceramics with a distorted rhombohedral crystal structure," Appl. Phys. Lett., vol. 87, pp. 262907 (3 pages), December 2005.

[9] K. Singh, R.K. Kotnala, and M. Singh, "Study of electric and magnetic properties of $(Bi_{0.9}Pb_{0.1})$ $(Fe_{0.9}Ti_{0.1})O_3$ nanomultiferroic system," Appl. Phys. Lett., vol. 93, pp. 212902 (3 pages), November 2008.

[10] S. Karimi, I.M. Reaney, I. Levin, and I. Sterianou, "Nd-doped $BiFeO_3$ ceramics with antipolar order," Appl. Phys. Lett., vol. 94, pp. 112903 (3 pages), March 2009.

[11] P. Pandit, S. Satapathy, P.K. Gupta, and V.G. Sathe, "Effect of coalesce doping of Nd and La on structure, dielectric, and magnetic properties of $BiFeO_3$," J Appl. Phys., vol. 106, pp. 114105 (7 pages), December 2009.

[12] V.L. Mathe, K.K. Patankar, R.N. Patil, and C.D. Lokhande, "Synthesis and dielectric properties of $Bi_{1-x}Nd_xFeO_3$ perovskites," J. Magn. Magn. Mater., vol. 270, 380-388, April 2004.

[13] G.L. Yuan, S.W. Or, J.M. Liu, and Z.G. Liu, "Structural transformation and ferroelectromagnetic behavior in single-phase $Bi_{1-x}Nd_xFeO_3$ multiferroic ceramics," Appl. Phys. Lett., vol. 89, pp. 052905 (3 pages), August 2006.

[14] T.-H. Wang, C.-S. Tu, H.-Y. Chen, Y. Ding, T.C. Lin, Y.-D. Yao, V. H. Schmidt, and K.-T. Wu, "Magnetoelectric coupling and phase transition in $BiFeO_3$ and $(BiFeO_3)_{0.95}(BaTiO_3)_{0.05}$ ceramics," J. Appl. Physics, vol. 109, pp. 044101 (4 pages), February 2011.

[15] V.H. Schmidt, G.F. Tuthill, C.-S. Tu, T.V. Schogoleva, and S.C. Meschia, "Random barrier height model for phase shifted conductivity in perovskites," Ferroelectrics, vol. 199, pp.51-67, July 1997.